Negative capacitors and inductors in optical plasmonic nanocircuits

Xu Qin,[1] Wangyu Sun,[1] Yijing He,[2] Ziheng Zhou,[1] and Yue Li[1,3,*]

[1]*Department of Electronic Engineering, Tsinghua University, Beijing 100084, China*

[2]*School of Information and Electronics, Beijing Institute of Technology, Beijing 100091, China*

[3]*Beijing National Research Center for Information Science and Technology, Beijing 100084, China*

(Received 29 May 2022; revised 6 September 2022; accepted 27 September 2022; published 10 October 2022)

Optical plasmonic nanocircuits are a heuristic route inspired by electronics for light manipulation in deep-subwavelength scales at optical frequencies with lumped capacitors and inductors. Here, a class of negative capacitors and inductors is discovered in the paradigm of optical plasmonic nanocircuits based on a modified model of a plasmonic nanoparticle. In this model, the global electromagnetic response of a Drude-dispersive plasmonic nanoparticle is imitated by a parallel pair of a capacitor and an inductor by involving the host medium of the plasmonic nanoparticle. We theoretically and numerically demonstrated the performance of such negative optical elements for extremely wideband impedance matching. A comprehensive lumped-element map for optical plasmonic nanocircuits is thus constructed including positive/negative inductors/capacitors with series/parallel configurations, which will inspire more possibilities in nanocircuit design.

DOI: 10.1103/PhysRevB.106.165410

I. INTRODUCTION

Plasmonic materials with the intrinsic Drude-like dispersion provide a negative permittivity in optical frequencies for light-matter interactions in deep-subwavelength scales [1–4]. Owing to the unprecedented abilities in light confinement and scattering, a variety of plasmonic nanostructures has been engineered for resonance and concentration [5–10], irregular optical responses [11–13], light transmission [14–18], optical lenses or nanoantennas [19–22], and other areas. Optical plasmonic nanocircuits are fascinating applications of plasmonics and introduce distinctive techniques originated in electronics at optical frequencies [23]. Analogous to the circuit theory in electronics, the plasmonic nanostructures are modeled by lumped elements such as nanoresistors, nanocapacitors, and nanoinductors. In contrast to traditional optical devices with electrically large dimensions, these plasmonic nanocircuits allow the modularization of light-matter interactions in deep-subwavelength scales, thus making it possible to operate as lumped circuits at optical frequencies. Therefore, versatile applications are proposed in this paradigm of nanocircuits by transplanting the classic techniques of electronics to optics and photonics, such as optical inductors and capacitors [24–26], optical filters [27–31], optical antennas impedance matching [32–34], optical Wheatstone bridge [35], and photoelectric computation [36].

The air background is applied in the resonance and scattering analysis of a plasmonic nanoparticle as a host medium in plasmonic nanocircuits [23]. However, it is important to include different host media in addition to air, considering the different host platforms of plasmonic nanocircuits. For this consideration, the general model of a plasmonic nanostructure can be expanded to a comprehensive one with different host media. As a result, the interaction between a plasmonic nanoparticle and its impinging light is imitated with a parallel capacitor and inductor pair, as shown in Fig. 1. Based on this model, we find that the host medium introduces an extra degree of freedom in light-scattering control and allows one to obtain negative capacitors and inductors. Theoretical and numerical verification was used to construct a map of lumped circuit elements in optical frequencies with both capacitors and inductors with positive/negative values and series/parallel configurations. These elements expand the paradigm of optical plasmonic nanocircuits and provide more possibilities in nanophotonic device design.

II. RESULTS

As the basic schema of optical plasmonic nanocircuits, a plasmonic nanoparticle has a homogeneous relative permittivity of ε_e and is positioned in the air [23]. Figure 1 shows that this nanoparticle is immersed in a host medium with relative permittivity of ε_h instead of the air. This nanoparticle has a deep-subwavelength dimension, which implies that the phase of impinging light is nearly constant over the nanoparticle. For the uniform incident electric field $\mathrm{E}_0 = E_0\hat{z}$ (the time convention $e^{-i\omega t}$ is assumed), the electric potential inside the nanoparticle is written as $\phi_{in} = -3\varepsilon_h E_0|\mathbf{r}|\cos\theta/(\varepsilon_e + 2\varepsilon_h)$ in spherical coordinates [37], where $\mathbf{r}$ is the position vector and θ is the angle between the position vector and the z axis. The nanoparticle's impedance can be derived as

$$Z = \frac{1}{-i\omega\pi R(\varepsilon_e - \varepsilon_h)\varepsilon_0/2}, \tag{1}$$

where R is the radius of the nanoparticle. The detailed derivation of (1) is presented in the Supplemental Material [38]. The impedance of the nanoparticle is clearly dependent on both

*lyee@tsinghua.edu.cn

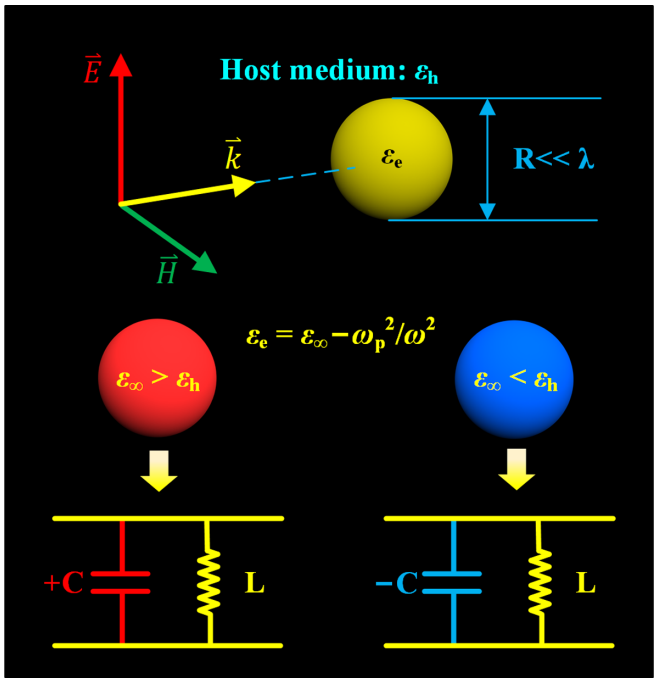

FIG. 1. Comprehensive lumped circuit model for a plasmonic nanoparticle. A Drude-dispersive nanoparticle immersed in the host medium with ε_h is modeled as parallel lumped circuit element pair of a capacitor (positive or negative depending on the host medium) and a positive inductor.

values of ε_e and ε_h. Specifically, when the relative permittivity of the nanoparticle is described by the Drude model, i.e., $\varepsilon_e = \varepsilon_\infty - \omega_p^2/\omega^2$ (ε_∞ is the relative permittivity at infinite frequency, and ω_p is the plasma frequency), the nanoparticle's impedance is written as follows:

$$Z = \frac{1}{-i\omega\pi R(\varepsilon_\infty - \varepsilon_h)\varepsilon_0/2 - \pi R\omega_p^2\varepsilon_0/(2i\omega)} = \frac{1}{-i\omega C - 1/(i\omega L)}. \quad (2)$$

The plasmonic nanoparticle's impedance could thus be described as a parallel capacitor with a capacitance of $C = \pi R(\varepsilon_\infty - \varepsilon_h)\varepsilon_0/2$ and a parallel inductor with an inductance of $L = 2/(\pi R\omega_p^2\varepsilon_0)$ in the theory of optical plasmonic nanocircuits [23], where the host medium is just air, and one nanoparticle is modeled via only one specific lumped positive capacitor or positive inductor. A more comprehensive model is established for plasmonic nanoparticles in (2) by incorporating the host media, which in turn provides a global understanding of the light-matter interaction from low to high frequencies. According to (2), the capacitance is dependent on both the permittivity of the nanoparticle and the host medium, which implies that the host medium provides a degree of freedom to tune this impedance. Specifically, when $\varepsilon_\infty > \varepsilon_h$, the capacitor in this model is just a regular capacitor with a positive capacitance. However, the capacitance has a negative value for the case of $\varepsilon_\infty < \varepsilon_h$, thus indicating a negative capacitor achieved by this nanoparticle. Particularly, in such a parallel pair, the capacitor leads the dominant response at high frequencies while the inductor takes a major role at low frequencies. Therefore, the lumped circuit model is reduced to a single capacitor in the high-frequency region, while a single inductor could present the model in the low-frequency region. In the middle frequencies, these two elements both work effectively with different responses from the single-element model discussed previously [23].

Considering the practical integration of the optical plasmonic nanocircuits, the subwavelength-thick slabs are embedded in a certain host medium, as shown in Fig. 2. The Supplemental Material [38] shows that this thin slab follows a similar model as (1), and its impedance can be derived as

$$Z = \frac{1}{-i\omega(\varepsilon_e - \varepsilon_h)\varepsilon_0 t}, \quad (3)$$

where t is the thickness of the slab. If the relative permittivity ε_e of the slab is described by the Drude model, i.e.,$\varepsilon_e = \varepsilon_\infty - \omega_p^2/\omega^2$, then the slab's impedance is

$$Z = \frac{1}{-i\omega(\varepsilon_\infty - \varepsilon_h)\varepsilon_0 t - \omega_p^2\varepsilon_0 t/i\omega}. \quad (4)$$

Equation (4) also implies that the lumped circuit model is equivalent to a parallel capacitor with a capacitance of $C = (\varepsilon_\infty - \varepsilon_h)\varepsilon_0 t$ and a parallel inductor with an inductance of $L = 1/(\omega_p^2\varepsilon_0 t)$, which are also dependent on both permittivities of the plasmonic slab and the host medium. Specifically, when the plasmonic slab ($\varepsilon_\infty = 3.7$, without loss of generality) is embedded in the host medium with relatively low permittivity, e.g., $\varepsilon_h = \varepsilon_{air}$, the parallel capacitor in this model has a positive capacitance of $C = (\varepsilon_\infty - \varepsilon_{air})\varepsilon_0 t$. As Fig. 2(b) depicts, in region I (low-frequency region), the slab is equivalent to a single inductor. In region III (high-frequency region), the positive capacitor gradually plays the dominant role. In region II, however, the total susceptance (the imaginary part of Z^{-1}) of two elements passes across zero at a certain frequency, which corresponds to inductor-capacitor (LC) resonance at this frequency.

The situation would be totally different if the plasmonic slab ($\varepsilon_\infty = 3.7$) is immersed in a host medium with higher permittivity, such as silicon ($\varepsilon_{Si} = 11.9$). In the model of a plasmonic slab in a host medium of silicon, a negative capacitor with a capacitance of $C = -(\varepsilon_{Si} - \varepsilon_\infty)\varepsilon_0 t$ is obtained, as illustrated in Fig. 2(c). The negative capacitor and the positive inductor both have negative susceptance. In fact, as exhibited in Fig. 2(d), a single positive inductor and a single negative capacitor play the dominant part of the lumped circuit model in region I and region III, respectively. The two elements both work effectively in region II, and the susceptance keeps negative without passing across zero, thus showing a different response, as can be seen in Fig. 2(b). The two cases above have different host media and therefore have different electromagnetic responses. The susceptance of the plasmonic slab is consistent between analytical and numerical results, thus providing the validity of this modified dual-element circuit model of plasmonic nanostructures. As shown in the derivation of Eq. (3), the circuit model is applicable when the thickness of the plasmonic slab is far smaller than the

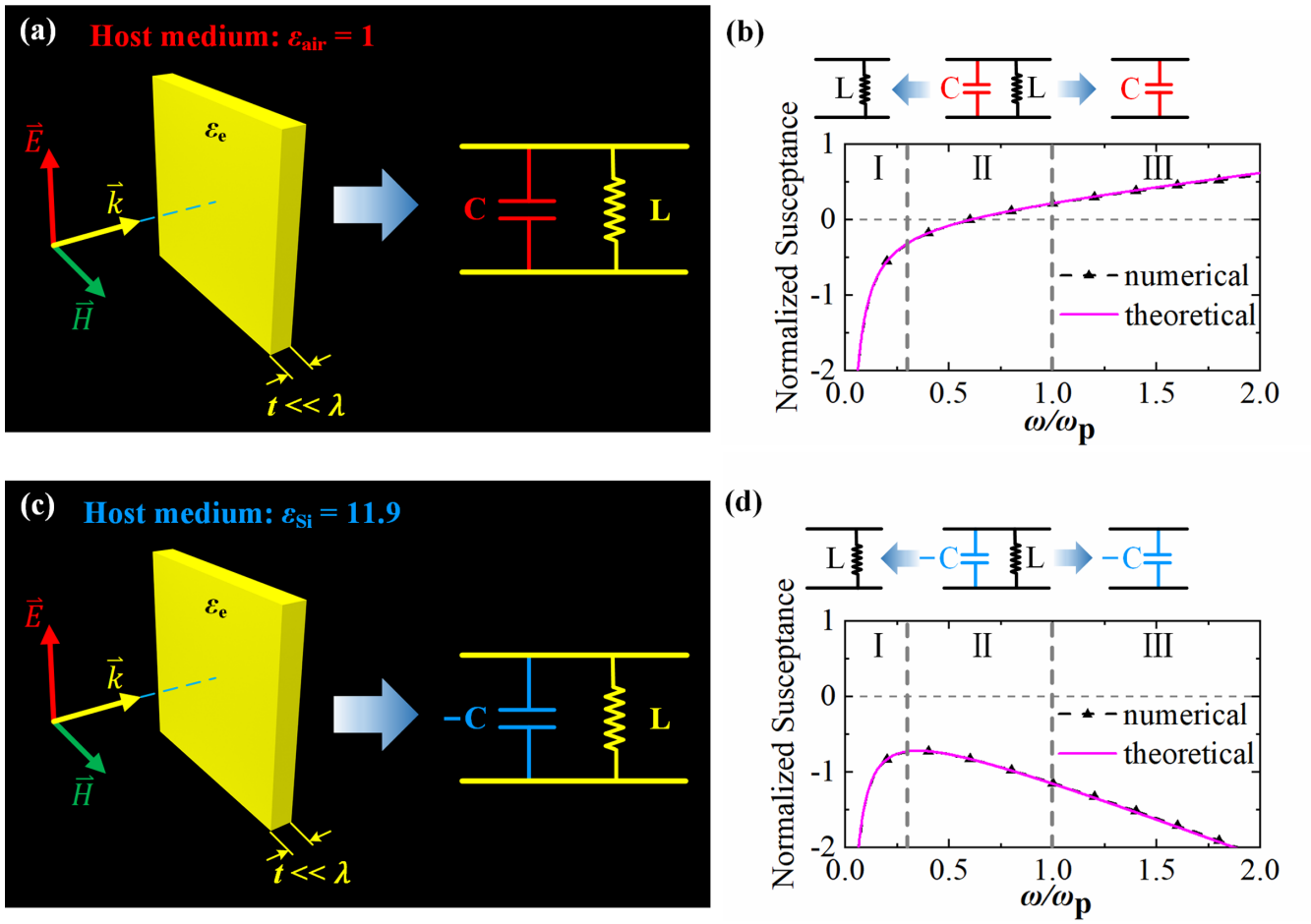

FIG. 2. Comprehensive lumped circuit model for a plasmonic slab with host media of air and silicon. (a), (c) Equivalent lumped circuits for plasmonic slabs with Drude dispersion $\varepsilon_e = \varepsilon_\infty - \omega_p^2/\omega^2$, in which ε_∞ is chosen to be a typical value of 3.7, and the thickness t is set to be $0.02\lambda_p$. The slab is immersed in the host medium of air and silicon, realizing positive and negative capacitors in the circuit models. (b), (d) Susceptance for the lumped circuits in the host medium of air and silicon; the model is reduced to a single inductor at low frequencies or a single capacitor at high frequencies. The susceptance is normalized by Z_{air}^{-1}, where Z_{air} is the intrinsic impedance of air $\sqrt{\mu_0/\varepsilon_{air}\varepsilon_0}$.

operating wavelength. Therefore, as the frequency increases, the error between the numerical and theoretical results gradually becomes larger, which can be seen in Figs. 2 (b) and 2(d).

As discussed above, the involvement of the host media adds extra degrees of freedom to tailor the impedance of the plasmonic nanostructures. Besides the positive capacitors and positive inductors which have been proposed in classical plasmonic nanocircuits, this model also indicates a negative capacitor in Figs. 2(c) and 2(d). Similar to their counterpart in electronics, negative circuit elements have a susceptance that is the opposite of positive elements, which can give them access to exotic functionalities for impedance matching [39–42]. Here, we demonstrate the application of negative circuit elements for extremely wideband impedance compensation. For this issue, an intuitive method to match a positive capacitor is to introduce a positive inductor. In this case, the impedance matching is only achieved within a narrow frequency range. The case will be different if we use a negative capacitor instead of a positive inductor. To illustrate this comparison, these two matching strategies are investigated with numerical verification. Figure 3(a) shows that the plasmonic slab behaves as a positive inductor with an inductance of $L = 1/(\omega_p^2 \varepsilon_0 t)$ in the low-frequency region. As depicted in Fig. 3(b), the total susceptance of the positive capacitor and the positive inductor equals zero only at the resonance frequency, which is expected to be $0.1\omega_p$. As a result, impedance matching is realized over a narrow frequency region around the resonance frequency.

However, for the same configuration but in the high-frequency region, the plasmonic slab behaves as a negative capacitor with a capacitance of $C = -(\varepsilon_{Si} - \varepsilon_\infty)\varepsilon_0 t$, as demonstrated in Fig. 3 (c).It is noted that in the low-frequency region, the plasmonic slab is effective to a single inductor and does not make sense in the matching by a negative capacitor. In this case, the total susceptance of the positive capacitor and the negative capacitor is close to zero for the high-frequency region from ω_p to $3\omega_p$, thus realizing impedance compensation within an extremely wide bandwidth, which is shown in Fig. 3(d). It is notable that the required positive inductor or negative capacitor could be analytically obtained in theoretical formulas without full-wave numerical simulation for a given positive capacitor, and the analytical design of the required lumped elements is validated by the numerical verification in Figs. 3(b) and 3(d). A detailed analysis is given in the Supple-

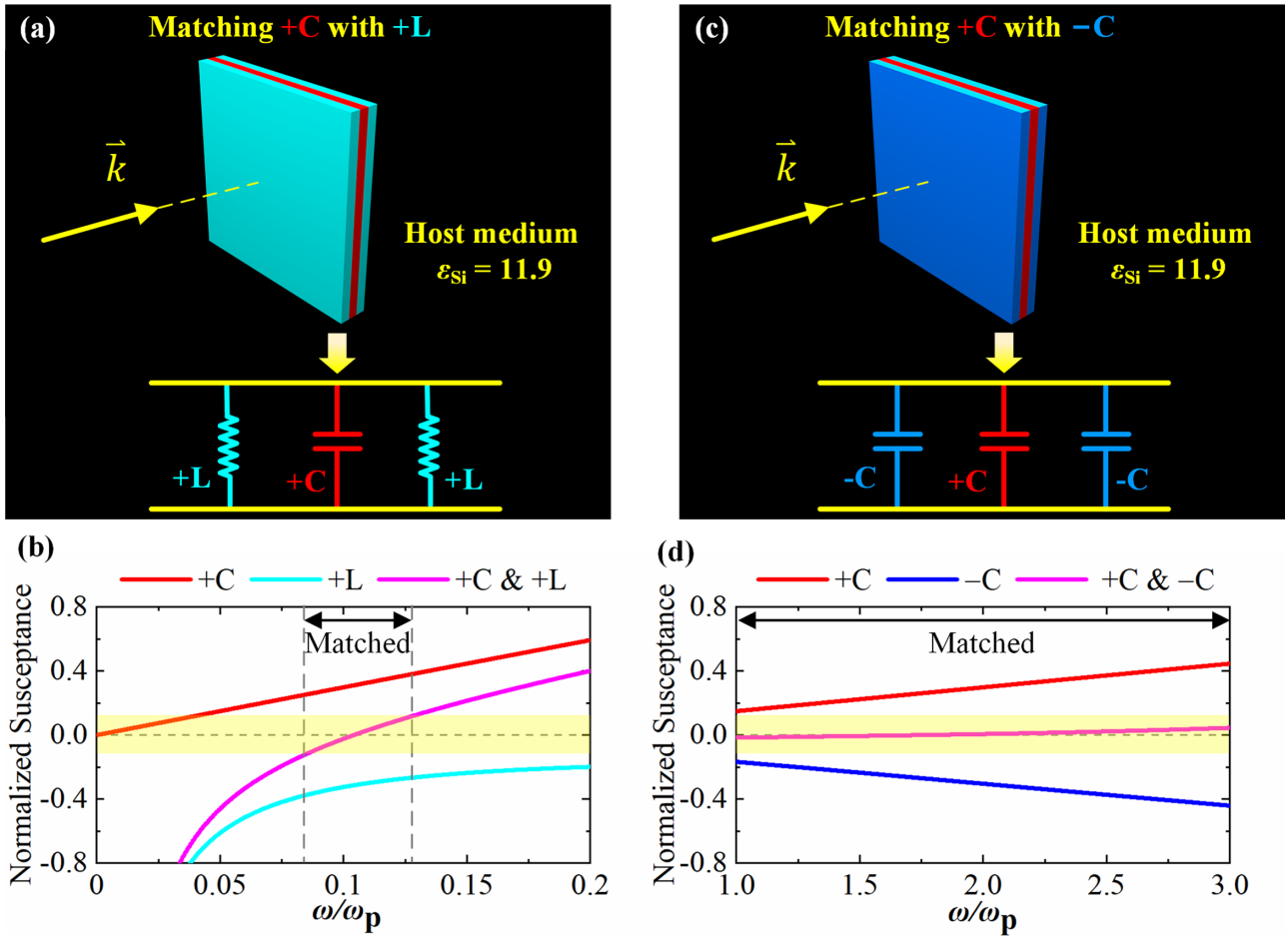

FIG. 3. Performance of impedance compensation of the positive capacitor with positive inductors and negative capacitors. Sketch of the positive capacitor with (a) positive inductor and (c) negative capacitor by introducing the slabs with Drude dispersion $\varepsilon_e = \varepsilon_\infty - \omega_p^2/\omega^2 (\varepsilon_\infty = 3.7)$. (b), (d) Susceptance of the corresponding circuits, showing the impedance compensation performance of the two methods. The susceptance is normalized by Z_{Si}^{-1}, where Z_{Si} is the intrinsic impedance of silicon $\sqrt{\mu_0/\varepsilon_{Si}\varepsilon_0}$.

mental Material [38]. As shown in the derivation of Eq. (3), the circuit model is applicable when the thickness of the plasmonic slab is far smaller than the operating wavelength. Therefore, as the frequency increases, the error between the numerical and theoretical results gradually becomes larger, which can be seen in Figs. 2(b) and 2(d). Therefore, the wideband impedance matching would also collapse with the frequency increases.

III. DISCUSSION

In this context, we established a comprehensive dual-element model via Eq. (2) using a capacitor with a capacitance of $C = \pi R(\varepsilon_\infty - \varepsilon_h)\varepsilon_0/2$ and an inductor with an inductance of $L = 2/(\pi R\omega_p^2\varepsilon_0)$, which is different from the model of the elements in plasmonic nanocircuits reported previously [23]. Importantly, this modified model could be reduced to a single-element model at different frequency regions, as demonstrated in Fig. 2. As another interesting property, it is also possible for the model to be reduced to a single element at a fixed frequency, which agrees with the basic elements of classical optical nanocircuits. For example, for the plasmonic nanoparticle with relative permittivity of $\varepsilon_e = \varepsilon_\infty - \omega_p^2/\omega^2$ and the host medium of ε_h, the capacitor in the parallel pair equals zero if $\varepsilon_\infty = \varepsilon_h$, i.e., $\varepsilon_e - \varepsilon_h = -\omega_p^2/\omega^2$, and only the inductor is left over the entire frequency range. A nonplasmonic nanoparticle with a constant relative permittivity of ε_e, i.e., $\varepsilon_e - \varepsilon_h = \text{const.}$, behaves as a single capacitor in this model.

To further investigate the feasible circuit designs of optical plasmonic nanocircuits, a comprehensive map of possible lumped elements is displayed in Fig. 4, including capacitors and inductors with positive/negative values and series/parallel configurations. A nanoparticle with a relative permittivity of ε_e and the host medium of ε_h has an element type that is dependent on the relative permittivity difference of $\Delta\varepsilon = \varepsilon_e - \varepsilon_h$. Starting from the existing parallel positive capacitors and inductors with $\Delta\varepsilon = \text{const.} > 0$ and $\Delta\varepsilon = -\omega_p^2/\omega^2 < 0$ in classical optical plasmonic nanocircuits [23], we next implement the parallel negative capacitors by $\Delta\varepsilon = \text{const.} < 0$ and the negative inductors by $\Delta\varepsilon = \omega_p^2/\omega^2 > 0$, which are exactly symmetrical to the positive elements. Furthermore, as the duality form of the parallel inductors/capacitors, the series capacitors/inductors could be obtained by replacing permittivity with permeability. According to the duality theorem [37], for the nanoparticle with a relative permeability of μ_e and the host medium of μ_h, the series element

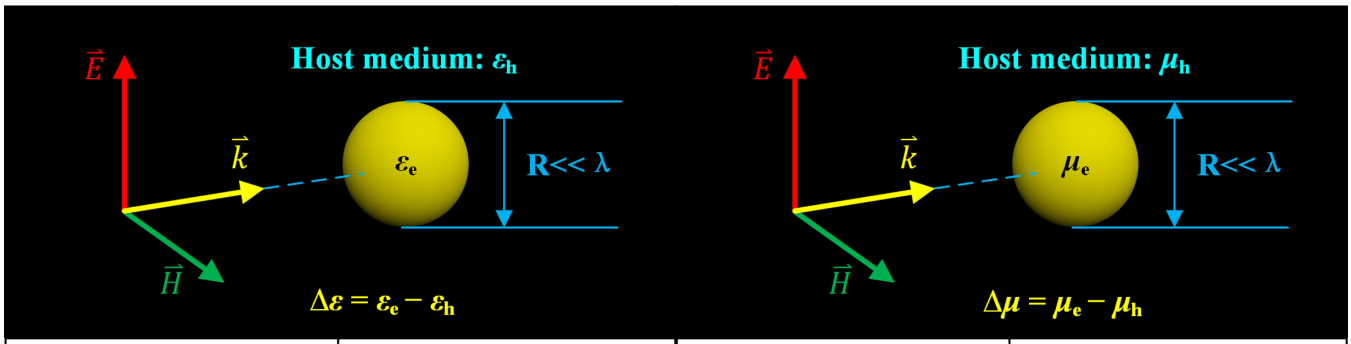

Parallel positive capacitor	Parallel positive inductor	Series positive inductor	Series positive capacitor
$\Delta\varepsilon = Const. > 0$ +C	$\Delta\varepsilon = -\omega_p^2/\omega^2 < 0$ +L	$\Delta\mu = Const. > 0$ +L	$\Delta\mu = -\omega_m^2/\omega^2 < 0$ +C
Parallel negative capacitor	**Parallel negative capacitor**	**Series negative inductor**	**Series negative capacitor**
$\Delta\varepsilon = Const. < 0$ −C	$\Delta\varepsilon = \omega_p^2/\omega^2 > 0$ −L	$\Delta\mu = Const. < 0$ −L	$\Delta\mu = \omega_m^2/\omega^2 > 0$ −C

FIG. 4. Map of the lumped elements in optical plasmonic nanocircuits, including realizations of positive and negative lumped elements for series or parallel configurations for expanded optical plasmonic nanocircuits.

type is dependent on the relative permeability difference of $\Delta\mu = \mu_e - \mu_h$. Concretely, the series positive inductors are realized by $\Delta\mu = \text{const.} > 0$, while the series positive capacitors are realized by $\Delta\mu = -\omega_m^2/\omega^2 < 0$, where ω_m is supposed to be magnetic plasma frequency. For the same relations, the series negative inductors and capacitors are obtained by $\Delta\mu = \text{const.} < 0$ and $\Delta\mu = \omega_m^2/\omega^2 > 0$, respectively, which are also symmetrical to the series positive inductors and capacitors. Therefore, a complete map of possible lumped elements in optical plasmonic circuits is established with corresponding material properties, as listed in Fig. 4.

To conclude, we investigated a modified but comprehensive circuit model for the plasmonic nanostructures by considering the host medium in optical plasmonic nanocircuits. The role of the host medium makes it possible to achieve negative capacitors or inductors, which are theoretically and numerically demonstrated for the extremely wideband impedance matching. Finally, a map of possible lumped elements for optical plasmonic nanocircuits is discussed with positive/negative capacitors/inductors with series/parallel configurations. Such a system exhibits exciting potential for the wideband impedance matching of antennas or circuits in optical frequencies.

IV. METHODS

A. Full-wave simulation

The theoretical results in Fig. 2 were derived by the software MATLAB. The numerical results in Fig. 2 and Fig. 3 were obtained using the frequency-domain solver of the commercial software CST STUDIO SUITE. The tetrahedral meshing was used with the meshing cells per max model box edge set to 10 for the model and 1 for the background. In the simulation, the waveguide ports were adopted to provide impinging light, and the numerical boundary setup for Fig. 2 and Fig. 3 was magnetic boundaries along the magnetic field and electric boundaries along the electric field to mimic light propagating in an open system.

The simulation data that support the findings of this study are available from the corresponding author upon reasonable request [38].

ACKNOWLEDGMENTS

This work was supported by the National Natural Science Foundation of China (NSFC) under Grant No. 62022045, and in part by the Beijing Nova Program of Science and Technology under Grant No. Z191100001119082.

[1] S. A. Maier, *Plasmonics: Fundamentals and Applications* (Springer, New York, 2007).

[2] W. L. Barnes, A. Dereux, and T. W. Ebbesen, Surface plasmon subwavelength optics, Nature (London) **424**, 824 (2003).

[3] S. A. Maier and H. A. Atwater, Plasmonics: Localization and guiding of electromagnetic energy in metal/dielectric structures, J. Appl. Phys. **98**, 011101 (2005).

[4] S. A. Maier, M. L. Brongersma, P. G. Kik, S. Meltzer, A. A. G. Requicha, and H. A. Atwater, Plasmonics—A route to nanoscale optical devices, Adv. Mater. **13**, 1501 (2001).

[5] S. Nie and R. E. Steven, Probing single molecules and single nanoparticles by surface-enhanced Raman scattering, Science **275**, 1102 (1997).

[6] C. Ciracì *et al.*, Probing the ultimate limits of plasmonic enhancement, Science **337**, 1072 (2012).

[7] N. Verellen *et al.*, Fano resonances in individual coherent plasmonic nanocavities, Nano Lett. **9**, 1663 (2009).

[8] B. Luk'yanchuk, N. I. Zheludev, S. A. Maier, N. J. Halas, P. Nordlander, H. Giessen, and C. T. Chong, The Fano resonance in plasmonic nanostructures and metamaterials, Nat. Mater. **9**, 707 (2010).

[9] X. Xu, S. Lin, Q. Li, Z. Zhang, I. N. Ivanov, Y. Li, W. Wang, B. Gu, Z. Zhang, C. H. Hsueh, P. C. Snijders, and K. Seal, Optical control of fluorescence through plasmonic eigenmode extinction, Sci. Rep. **5**, 9911 (2015).

[10] X. Meng, S. Liu, J. I. Dadap, and R. M. Osgood, Jr., Plasmonic enhancement of a silicon-vacancy center in a nanodiamond crystal, Phys. Rev. Mater. **1**, 015202 (2017).

[11] M. S. Tame, K. R. McEnery, Ş. K. Özdemir, J. Lee, S. A. Maier, and M. S. Kim, Quantum plasmonics, Nat. Phys. **9**, 329 (2013).

[12] H. Alaeian and J. A. Dionne, Non-Hermitian nanophotonic and plasmonic waveguides, Phys. Rev. B **89**, 075136 (2014).

[13] L. Persechini *et al.*, Optical characterisation of plasmonic nanostructures on planar substrates using second–harmonic generation, Opt. Express **23**, 26486 (2015).

[14] J. A. Dionne, L. A. Sweatlock, H. A. Atwater, and A. Polman, Planar metal plasmon waveguides: Frequency-dependent dispersion, propagation, localization, and loss beyond the free electron model, Phys. Rev. B **72**, 075405 (2005).

[15] R. Zia, M. D. Selker, P. B. Catrysse, and M. L. Brongersma, Geometries and materials for subwavelength surface plasmon modes, J. Opt. Soc. Am. A **21**, 2442 (2004).

[16] M. Silveirinha and N. Engheta, Tunneling of Electromagnetic Energy through Subwavelength Channels and Bends Using E-Near-Zero Materials, Phys. Rev. Lett. **97**, 157403 (2006).

[17] M. G. Silveirinha and N. Engheta, Theory of supercoupling, squeezing wave energy, and field confinement in narrow channels and tight bends using ε near-zero metamaterials, Phys. Rev. B **76**, 245109 (2007).

[18] A. Alù and N. Engheta, Light squeezing through arbitrarily shaped plasmonic channels and sharp bends, Phys. Rev. B **78**, 035440 (2008).

[19] M. W. Knight, H. Sobhani, P. Nordlander, and N. J. Halas, Photodetection with active optical antennas, Science **332**, 702 (2011).

[20] X. Ni, K. Emani Naresh, V. Kildishev Alexander, A. Boltasseva, and M. Shalaev Vladimir, Broadband light bending with plasmonic nanoantennas, Science **335**, 427 (2012).

[21] X. Ni, S. Ishii, A. V. Kildishev, and V. M. Shalaev, Ultra-thin, planar, Babinet-inverted plasmonic metalenses, Light: Sci. Appl. **2**, e72 (2013).

[22] D. Lin, P. Fan, E. Hasman, and L. Brongersma Mark, Dielectric gradient metasurface optical elements, Science **345**, 298 (2014).

[23] N. Engheta, A. Salandrino, and A. Alù, Circuit Elements at Optical Frequencies: Nanoinductors, Nanocapacitors, and Nanoresistors, Phys. Rev. Lett. **95**, 095504 (2005).

[24] A. Alù and N. Engheta, All Optical Metamaterial Circuit Board at the Nanoscale, Phys. Rev. Lett. **103**, 143902 (2009).

[25] B. Edwards and N. Engheta, Experimental Verification of Displacement-Current Conduits in Metamaterials-Inspired Optical Circuitry, Phys. Rev. Lett. **108**, 193902 (2012).

[26] M. G. Silveirinha, A. Alù, J. Li, and N. Engheta, Nanoinsulators and nanoconnectors for optical nanocircuits, J. Appl. Phys. **103**, 064305 (2008).

[27] H. Caglayan, S.-H. Hong, B. Edwards, C. R. Kagan, and N. Engheta, Near-Infrared Metatronic Nanocircuits by Design, Phys. Rev. Lett. **111**, 073904 (2013).

[28] H. Liu, Shivanand, and K. J. Webb, Optical circuits from anisotropic films, Phys. Rev. B **79**, 094203 (2009).

[29] Y. Sun, B. Edwards, A. Alù, and N. Engheta, Experimental realization of optical lumped nanocircuits at infrared wavelengths, Nat. Mater. **11**, 208 (2012).

[30] Y. Li, I. Liberal, and N. Engheta, Dispersion synthesis with multi-ordered metatronic filters, Opt. Express **25**, 1937 (2017).

[31] Q. Zhang, L. Bai, Z. Bai, P. Hu, and C. Liu, Equivalent-nanocircuit-theory-based design to infrared broad band-stop filters, Opt. Express **23**, 8290 (2015).

[32] A. Alù and N. Engheta, Tuning the scattering response of optical nanoantennas with nanocircuit loads, Nat. Photonics **2**, 307 (2008).

[33] J.-S. Huang, T. Feichtner, P. Biagioni, and B. Hecht, Impedance matching and emission properties of nanoantennas in an optical nanocircuit, Nano Lett. **9**, 1897 (2009).

[34] N. Liu, F. Wen, Y. Zhao, Y. Wang, P. Nordlander, N. J. Halas, and A. Alù, Individual nanoantennas loaded with three-dimensional optical nanocircuits, Nano Lett. **13**, 142 (2013).

[35] Y. Li, I. Liberal, and N. Engheta, Metatronic analogues of the Wheatstone bridge, J. Opt. Soc. Am. B **33**, A72 (2016).

[36] A. Silva, F. Monticone, G. Castaldi, V. Galdi, A. Alu, and N. Engheta, Performing mathematical operations with metamaterials, Science **343**, 160 (2014).

[37] J. D. Jackson, *Classical Electrodynamics*. 3rd ed. (John Wiley & Sons, Inc., New York, 1999).

[38] See Supplemental Material at http://link.aps.org/supplemental/10.1103/PhysRevB.106.165410 for theoretical derivation, detailed geometry of numerical analysis, and additional discussion.

[39] P. Y. Chen, C. Argyropoulos, and A. Alù, Broadening the Cloaking Bandwidth with Non-Foster Metasurfaces, Phys. Rev. Lett. **111**, 233001 (2013).

[40] M. M. Jacob and D. F. Sievenpiper, Non-Foster matched antennas for high-power applications, IEEE Trans. Antennas Propag. **65**, 4461 (2017).

[41] J. Mou and Z. Shen, Broadband and thin magnetic absorber with non-Foster metasurface for admittance matching, Sci. Rep. **7**, 6922 (2017).

[42] M. Alibakhshikenari *et al.*, Bandwidth and gain enhancement of composite right left handed metamaterial transmission line planar antenna employing a non Foster impedance matching circuit board, Sci. Rep. **11**, 7472 (2021).